Photodiagnosis and Photodynamic Therapy 25 (2019) 425–435

Contents lists available at ScienceDirect

Photodiagnosis and Photodynamic Therapy

journal homepage: www.elsevier.com/locate/pdpdt

# Modeling PpIX effective light fluence at depths into the skin for PDT dose comparison

Ethan P.M. LaRochelle[a,*], Kayla Marra[a], Robert E. LeBlanc[b], M. Shane Chapman[c], Edward V. Maytin[d], Brian W. Pogue[a,c]

[a] Thayer School of Engineering, Dartmouth College, Hanover, NH 03755, USA
[b] Department Pathology & Laboratory Medicine, Geisel School of Medicine, Dartmouth College, Lebanon, NH 03756, USA
[c] Department of Surgery, Geisel School of Medicine, Dartmouth College, Lebanon, NH 03756, USA
[d] Department of Biomedical Engineering, Cleveland Clinic, Cleveland, OH 44195, USA

ARTICLE INFO

*Keywords:*
Photodynamic therapy
Daylight PDT
PpIX-weighted light dose
Tissue optics
Monte Carlo

ABSTRACT

*Background:* Daylight-activated PDT has seen increased support in recent years as a treatment method for actinic keratosis and other non-melanoma skin cancers. The inherent variability observed in broad-spectrum light used in this methodology makes it difficult to plan and monitor light dose, or compare to lamp light doses.
*Methods:* The present study expands on the commonly used PpIX-weighted effective surface irradiance metric by introducing a Monte Carlo method for estimating effective fluence rates into depths of the skin. The fluence rates are compared between multiple broadband and narrowband sources that have been reported in previous studies, and an effective total fluence for various treatment times is reported. A dynamic estimate of PpIX concentration produced during pro-drug incubation and treatment is used with the fluence estimates to calculate a photodynamic dose.
*Results:* Even when there is up to a 5*x* reduction between the effective surface irradiance of the broadband light sources, the effective fluence below 250 μm depth is predicted to be relatively equivalent. An effective threshold fluence value (0. 70 $J_{eff}/cm^2$) is introduced based on a meta-analysis of previously published ALA-PpIX induced cell death. This was combined with a threshold PpIX concentration (50 nM) to define a threshold photodynamic dose of 0.035 u M $J_{eff}/cm^2$.
*Conclusions:* The threshold was used to generate lookup tables to prescribe minimal treatment times to achieve depth-dependent cytotoxic effect based on incubation times and irradiance values for each light source.

## 1. Introduction

Photodynamic therapy (PDT) for treatment of actinic keratosis (AK) and other non-melanoma skin cancers has been an approved clinical practice for decades [1–3], and just in the past few years daylight-activated PDT for AK has gained support as an approved treatment method [4–6]. With the shift from conventional PDT use of blue (415 nm) or red (633 nm) lamp sources, to daylight-PDT, where broadband sources like the sun or other artificial white lights have been explored, the complexity of light dose estimation is increased.

Prescribing a sufficient photodynamic dose requires knowledge of both how light interacts with tissue as well as how the clinical presentation can influence the tissue morphology. As clinical context for the current study, Fig. 1 shows histopathology examples of actinic keratosis (AK) and other non-melanoma skin cancers, where Table 1 provides the corresponding depth profile of each lesion. From these case examples it can be observed there is a range over which the photodynamic dose must be effective, and this dose will vary based on both PpIX production and light fluence reaching the entirety of the lesion. Yet, most treatments only consider the light dose at the skin surface.

While there have been proposed methods to estimate the spectrally-weighted light dose relative to the PpIX spectrum [4,7–10], these approaches do not account for the spectral attenuation in the skin. Using Monte Carlo modeling, the present study aims to provide clinically relevant methods to understand how surface irradiance measurements can be used to estimate the light fluence rate at depth in tissue, which should allow informed decisions about treatment time and appropriate light sources, thus improving the ability to tailor PDT treatments based on the clinical presentation of the disease.

* Corresponding author.
*E-mail address:* ethan.phillip.m.larochelle.th@dartmouth.edu (E.P.M. LaRochelle).

https://doi.org/10.1016/j.pdpdt.2019.01.022
Received 19 September 2018; Received in revised form 4 January 2019; Accepted 18 January 2019
Available online 25 January 2019
1572-1000/ 

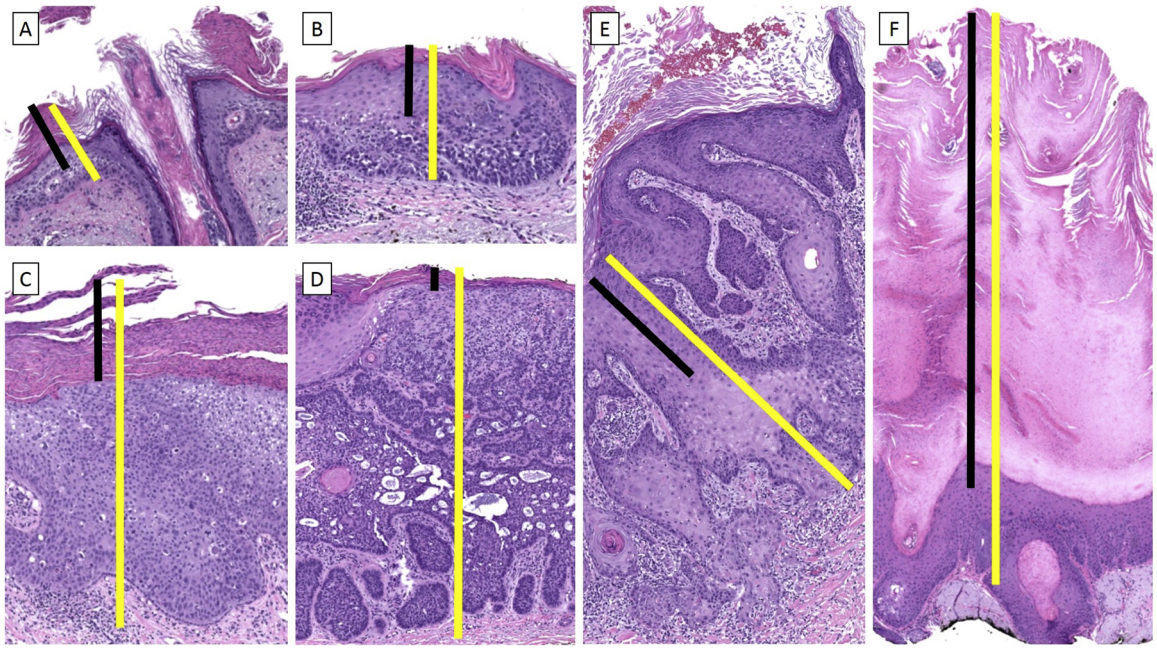


**Fig. 1.** Representative skin lesions (H&E 40×). The black line represents the distance from the surface of the corneal layer to the surface of the lesion. The yellow line represents the distance from the surface of the corneal layer to the base of the lesion. An example of an actinic keratosis (A), basal cell carcinoma, superficial type (B), squamous cell carcinoma in situ (C), basal cell carcinoma, nodular type (D), invasive well-differentiated squamous cell carcinoma (E), and a hypertrophic actinic keratosis (F).

**Table 1**
Depths of Representative Skin Lesions from Fig. 1.

| | Measurement from surface of corneal layer to surface of lesion (μm) | Measurement from surface of corneal layer to base of lesion (μm) |
|---|---|---|
| (A) Actinic keratosis | 189 | 222 |
| (B) Hypertrophic actinic keratosis | 1419 | 1708 |
| (C) Squamous cell carcinoma in situ | 305 | 1038 |
| (D) Invasive squamous cell carcinoma | 287 | 692 |
| (E) Basal cell carcinoma, superficial type | 214 | 403 |
| (F) Basal cell carcinoma, nodular type | 70 | 1108 |

In Europe, Metvix® or MAL is the common form of ALA used for topical PDT, whereas Levulan® is used in the United States [2]. More recently, Ameluz® has been approved in both markets for treatment of AK and tissue debridement. MAL-equivalent Luxerm® and Ameluz® are also approved in Europe for daylight-PDT. For conventional lamp activated PDT, all formulations are applied and let to incubate for a period on the order of hours and then activated with a blue (415 nm 10–25 J/cm$^2$) [11,12] or red (633 nm, 37 −125 J/cm$^2$) [13,14] light. But, in the daylight PDT protocol, this can differ slightly depending on the drug formulation, but generally the incubation is minimized to be near 30 min and the activation solar irradiance is much lower [4,8,10,15–18]. In conventional PDT, the PpIX production has been reported to penetrate up to depths of 2 mm with 3 h incubation [19], whereas during daylight-PDT PpIX is thought to be produced continuously during the treatment [4,5,7,15,20] and few reports on depth are known. The shorter ALA incubation time combined with the lower irradiance and longer PpIX activation time is thought to be the driving factor in reports of lower pain with daylight PDT [4,16,21,22].

The spectral characteristics of light dictate the depth of potential PpIX activation. Due to tissue optical properties blue light will have a much more superficial activation profile than red light. However, PpIX has peak absorption in the blue (˜410 nm), but also in Q-bands at 505 nm, 540 nm, 580 nm and 635 nm [23,24]. Optimizing these factors, depth of activation and peak absorption, can be easily accomplished with narrowband light sources such as LEDs by altering the irradiance. This optimization becomes slightly more challenging when broad-spectrum light sources are used, especially when using a natural light source such as the sun. The consensus method for comparing broad-spectrum light sources is to weight the measured spectrum by the normalized PpIX spectrum resulting in a measure of effective irradiance [4,7–10]. Briefly, this is accomplished by first measuring the spectrally resolved irradiance at the skin surface (Fig. 2A). This spectrum is then multiplied by a normalized PpIX absorption spectrum, [24] resulting in a measure of effective irradiance (Fig. 2B). The effective irradiance provides a weighting factor for the probability of PpIX activation so that different light sources can be more easily compared. However, in the presence of tissue attenuation, the light fluence rate will vary drastically as a function of both wavelength and depth.

Previous Monte Carlo studies have investigated the interactions of light, tissue and PpIX from a variety of perspectives. Comparisons of clinical fluorescence measurements with tissue models have been used to estimate the depth distribution of PpIX [25]. Expanding on this idea, a model using three excitation sources was developed to study the oxygen concentration and resulting reactive oxygen caused by PpIX activation [26]. The most similar work to the present study was conducted by Campbell et al., who modeled both daylight and red-light activation of PpIX for a skin tumor model, and in subsequent work modeled the continuous production of PpIX during both conventional and daylight-PDT treatment [20,27]. The work presented here expands on the previous studies by using a 7-layer skin model with the ability to

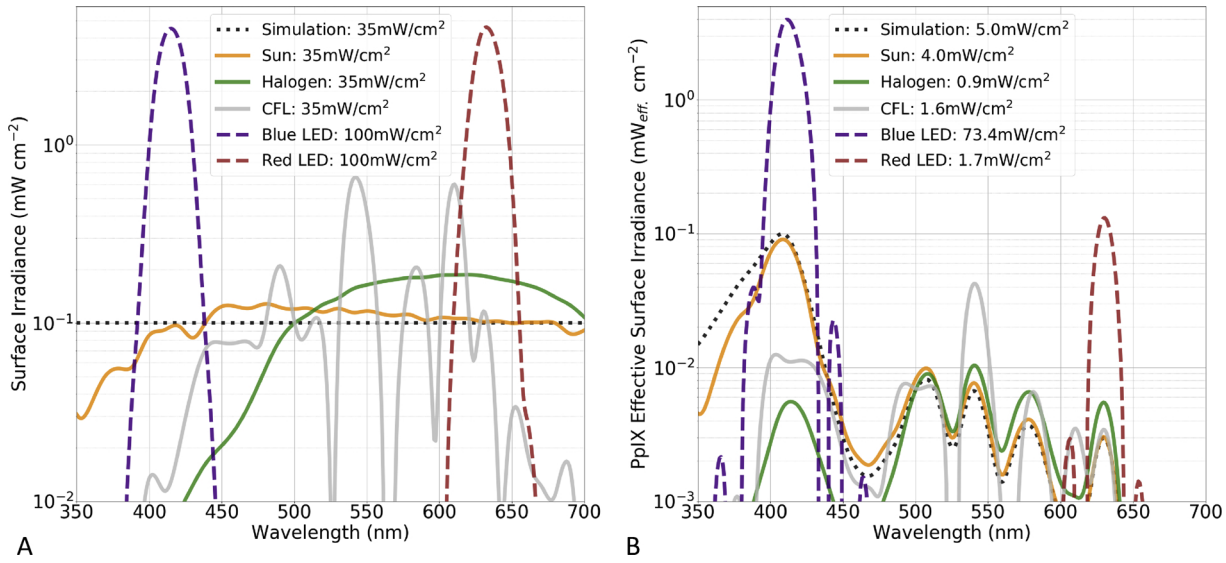


**Fig. 2.** (A) Spectrum of 6 light sources. The simulation (dotted) is based on a theoretical uniform spectrum, whereas the other white light sources (solid) are of equal irradiance but based on measured spectral distributions. The narrow-band sources (dashed) are based on clinically-relevant irradiance used in conventional PDT and the spectrum is nearly equivalent to the FDA-approved Blue-U (Sun/DUSA) and the RhodaLED (Biofrontera) light sources. (B) PpIX-weighted spectrum showing wide variation in effective irradiance.

Monte Carlo model any light source in the 350–900 nm spectral range at 10 nm spectral resolution. The resulting light fluence information is then combined with estimates of PpIX production and photobleaching as well as light fluence thresholds to tabulate clinically-relevant treatment times based upon the applied light source and the desired depth of activation in tissue.

A simplified model to determine the potential for PpIX activation may consider only light fluence in tissue, which assumes a sufficient and uniform distribution of PpIX. However, recent models have shown the importance of accounting for PpIX distribution when determining the photodynamic dose [20,25–27]. As such, estimates of PpIX distribution have been considered using both incubation times of 30 min or less, commonly used in daylight-PDT protocols, and incubation times of over an hour which better represent conventional-PDT. Since the irradiance used in these protocols cover a wide range, photobleaching will occur over differing time-scales. The present model assumes oxygen concertation remains sufficient throughout the treatment period.

## 2. Materials and methods

### 2.1. Monte Carlo model

Using the Monte Carlo software GAMOS [28,29], a 7-layer skin model (Figs. 3 and 4) was defined based on the work of Meglinski [30]. Tissue optical properties ($\mu_a$, $\mu_s$, g, n) were defined between 350 nm–900 nm at a 10 nm spectral spacing (Fig. 3 and Supplementary Data: S1) using the tissue-optics plugin for GAMOS [31]. The tissue optical properties assume lightly pigmented skin, which correspond to approximately 1% melanin in the epidermis (Skin layer 2 in Fig. 3). A custom Python script (S2) converted the input file (S1) into a baseline template for a GAMOS geometry file. The total tissue volume was placed in a 20 cm x 20 cm x 2 cm box where the top 7.9 mm contained the explicitly defined skin model. A voxelized parallel geometry was defined with 1 cm × 1 cm × 10 µm voxels within the skin to measure the fluence. A 5 cm diameter disc-shaped light with 1° divergence was modeled as the source 60 mm above the skin surface. The voxelized geometry is only defined as a single XY volume per 10um Z-step to reduce the analysis complexity. The overall XY dimensions of the tissue volume are much larger than the voxelized geometry to better simulate a semi-infinite slab geometry. PpIX absorption is not considered in the current model, since it is assumed the concentration would not be large enough to have a substantial impact on the overall tissue optical properties [25]. Simulations were run using $10^7$ photons for each of the defined wavelengths.

The simulations were run using Amazon Web Services (AWS) Batch service. Briefly, a simulation template was created and uploaded to and AWS S3 bucket. This template contained a zip file (S3) with the necessary input files and a bash script that processed simulation input arguments (source wavelength, number of photons, and random seed). An AWS Batch job definition was generated programmatically, which specified compute parameters for each simulation job (1–3 virtual CPUS, and 2000-4000MB memory). The jobs were then added to the queue and run in parallel using AWS EC2 instances (c4.large – c4.8xlarge). Simulation outputs were stored in sub-directories of the S3 Bucket and retrieved using the AWS command line interface for analysis on a local computer. All analysis was done using custom Python scripts (S2).

### 2.2. Light fluence

The following sections compare narrowband blue and red light at clinically relevant surface irradiance with broadband sources that have been reported in previous daylight and low-fluence-rate PDT models [10,18]. The narrow-band sources are modeled based on clinically available sources, such as the Blue-U (Sun/DUSA) and the RhodaLED (Biofrontera). The broadband sources are based on measurements taken by a spectroradiometer (Apogee SS-110), as reported previously [18].

Like the PpIX effective surface irradiance, the effective fluence rate was calculated by weighting the fluence rate by the PpIX absorption spectrum. Using the PpIX-weighted effective fluence rate at various depths in tissue, the effective light dose could then be determined for each source.

In broad-spectrum PDT applications, the effective light dose is often reported as a product of the normalized PpIX absorption spectrum and the source spectrum [4,7–10]. This idea was applied to the fluence rate estimates by first taking the idealized case where each modeled wavelength had the same number of photons ($10^7$), and then extended to match measured light sources by first weighting the model by the measured spectrum (1) and then applying the PpIX absorption

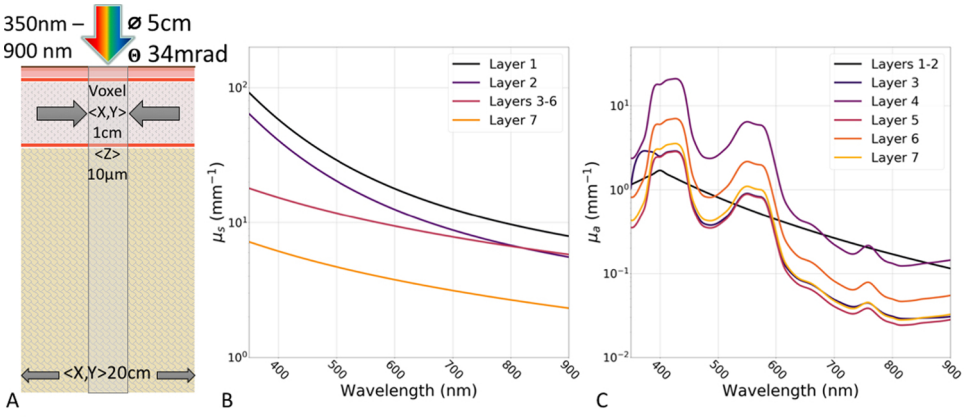


| | Layer 1 (Stratum corneum) | Layer 2 (Living epidermis) | Layer 3 (Papillary dermis) | Layer 4 (Upper blood net dermis) | Layer 5 (Reticular dermis) | Layer 6 (Deep blood net dermis) | Layer 7 (Subcu. fat) |
|---|---|---|---|---|---|---|---|
| n | 1.50 | 1.34 | 1.40 | 1.39 | 1.40 | 1.38 | 1.44 |
| g | 0.86 | 0.80 | 0.90 | 0.95 | 0.80 | 0.95 | 0.75 |

**Fig. 3.** A representation of the GAMOS geometry is shown in the upper left. Tissue optical properties $\mu_s$ (middle) and $\mu_a$ (right) were defined between 350 nm and 900 nm for each of the 7 tissue layers. A constant refractive index (n) and anisotropy (g) were assumed for each layer and are provided in the table.

weighting (2). The estimated spectral fluence rate at depth z, was:

$$\phi(\lambda, z)\left(mW/cm^2\right) = E_{meas}(\lambda, 0)*\phi_{model}(\lambda, z) \quad (1)$$

Where $E_{meas}$ is the spectrally measured irradiance at the surface and $\varphi_{model}$ is the spectral attenuation due to tissue as modeled for the defined wavelength ($\lambda$) at depth z.

Then the effective spectral fluence rate was calculated as:

$$\phi_{eff}(\lambda, z)\left(mW_{eff}/cm^2\right) = E_{meas}(\lambda, 0)*\phi_{model}(\lambda, z)*A_{PpIX}(\lambda) \quad (2)$$

Where $A_{PpIX}$ is the normalized spectral attenuation of PpIX.

The effective fluence is the product of the effective fluence rate and the treatment time. The effective threshold fluence is based on previously reported fluence values for studies using at least 0.6 mM ALA and a laser or LED light source [32–34], as summarized by Gonçalves de Faria (Table 2) [35]. Since the wavelength for each study was reported for each cytotoxic probability distribution with mean fluence ($D_P$) and FWHM of the distribution ($\Delta D$) [35], the equivalent effective fluence could then be calculated using the PpIX absorption spectrum weighting (3–5).

$$\zeta_\lambda = \int_{\mu-3\sigma}^{\mu+3\sigma} A_{PpIX}(\lambda)d\lambda \quad (3)$$

$$D_{P,\,eff} = \zeta_\lambda D_P \quad \sigma_{D,\,eff} = \zeta_\lambda \sigma_D \quad (4)$$

$$\sigma_{D,\,eff,pooled} = \sqrt{\frac{\sum \sigma_{D,n}}{N}} \quad (5)$$

Where $A_{PpIX}$ is again the normalized spectral attenuation of PpIX over the wavelength range of interest and $\sigma_D$ is the standard deviation calculated from the probability distribution $\Delta D$.

### 2.3. PpIX production and photobleaching

Since the Monte Carlo model only considers light fluence, and not PpIX production or photobleaching, Python scripts (S2) were developed to perform this portion of the analysis. PpIX production was estimated based on the model that is well summarized by Campbell et al. [20] and the parameters used in this study match those presented by Campbell. Briefly, the PpIX concentration is based on the diffusion rate of the pro-drug (6), and the rate and efficiency the drug is converted to PpIX (7).

The pro-drug concentration M is first calculate at depth z and time t using:

$$M(z, t) = M_0\left(1 - erf\left(\frac{z}{\sqrt{4Dt}}\right)\right) \quad (6)$$

Where $M_0$ is the initial concentration of the pro-drug applied to the surface (z = 0) at time t = 0 and is assumed to be $6 \times 10^{16}$ cm$^{-3}$. D is the diffusion coefficient and assumed to be $6.9 \times 10^{-7}$ cm$^2$ s$^{-1}$. The resulting PpIX production at depth z and time t can be calculated using:

$$P(z, t) = \frac{\varepsilon_p}{\tau_{ap}}\int_0^t e^{-\frac{t-t'}{\tau_p}} M(z, t')dt' \quad (7)$$

Where $\varepsilon_p$ is the yield or proportion of pro-drug converted to PpIX, which is assumed to be 0.5, and $\tau_{ap}$ is the relaxation time or rate of conversion of the pro-drug and is assumed to be 8640 s. The rate of PpIX clearance is reflected in $\tau_p$ and is assumed to be 4680 s. The result of this calculation is the number of PpIX molecules per cubic centimeter. In the current study, this was converted to molar concentration to allow for better comparison with clinical findings.

Photobleaching was estimated as a simple exponential decay based on the initial PpIX concentration and fluence rate [20,25,27], but with two modifications:

$$C(z, t) = C_0(z)e^{-\phi_{eff}(z)t/\beta} \quad (8)$$

first, $\varphi_{eff}(z)$ is the PpIX-weighted effective fluence, and second, the photobleaching dose constant (ß) is calculated for the peak PpIX absorption at 410 nm (0.65 J cm$^{-2}$) using the method presented by Campbell to determine the wavelength-dependent photobleaching dose constant, assuming ß(630 nm) to be 14 J cm$^{-2}$, as reported by Valentine[25]. $C_0(z)$ is the initial PpIX concentration at the specified depth, z.

PpIX concentrations resulting from different incubation periods, when light is assumed to be negligible, are first calculated using Eqs. 6 and 7. Then, both PpIX production and photobleaching must be considered during the light treatment phase. The PpIX concentration at depth is updated iteratively to account for both processes during treatment.

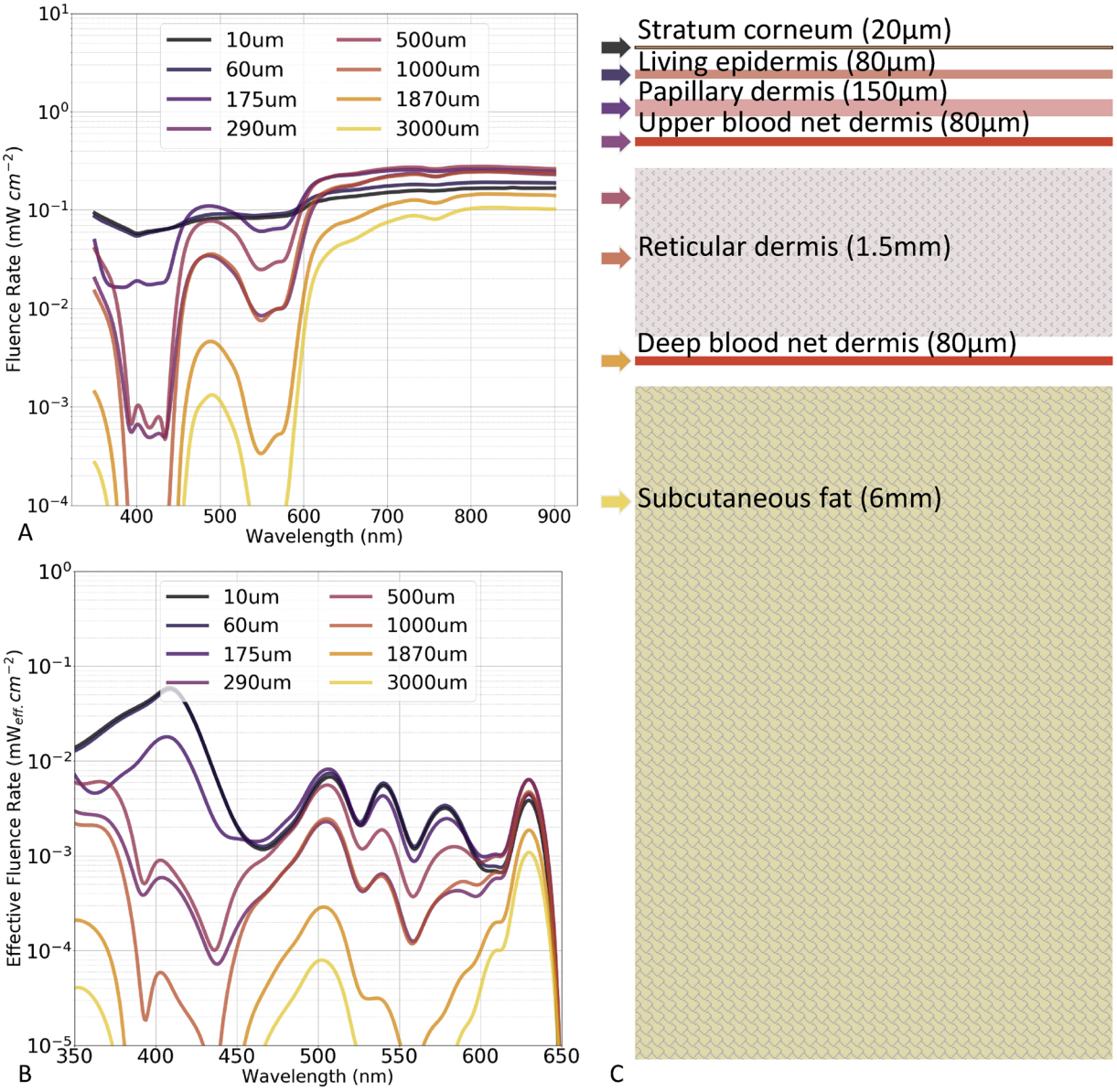


**Fig. 4.** (A) Fluence rate at various depths in 7-layer tissue model, based on a simulated spectrally uniform light source. (B) The PpIX-weighted effective fluence rate in the same model. (C) Geometry of 7-layer skin model, where arrows indicate depths used in A and B.

**Table 2**
Light dose distribution parameters used to calculate effective cytotoxic threshold.

| Wavelength (nm) | 405 | 405 | 514 | 514 | 630 | 634 |
|---|---|---|---|---|---|---|
| $D_P$ (J/cm$^2$) | 0.14 | 0.14 | 0.16 | 1.11 | 0.79 | 1.54 |
| $\sigma_D$(J/cm$^2$) | 0.13 | 0.13 | 0.09 | 0.24 | 0.27 | 1.49 |
| $D_{P,\,eff}$(J$_{eff}$/cm$^2$) | 0.12 | 0.12 | 0.01 | 0.07 | 0.01 | 0.03 |
| $\sigma_{D,\,eff}$(J$_{eff}$/cm$^2$) | 0.11 | 0.11 | 0.01 | 0.01 | 0.01 | 0.02 |

### 2.4. Photodynamic dose

Initial incubation times of 5, 30, 60, and 120 min were assumed. For each light source the fluence rate at depths in tissue was linearly scaled to represent a range of surface irradiance values. Through iteratively calculating the PpIX distribution based on these input parameters, the photodynamic dose can be determined over a range of times and resulting effective fluence values. An effective photodynamic dose is defined as the product of the threshold effective fluence and a PpIX concentration of 50 nM.

## 3. Results

Using the normalized PpIX absorption spectrum as a weighting factor is common method to compare the effective irradiance of different broadband light sources. For the light sources considered in the present work, even though the broadband sources have an equal irradiance, the PpIX-effective irradiance demonstrates up to a 5*x* difference (Fig. 2). Similarly, the blue and red LED sources have respective effective fluence rates of just 73% and 2% of the unweighted values

While PpIX-weighting improves the ability to compare surface irradiance, it does not consider tissue optical properties. Fig. 4A shows how the fluence rate of a spectrally uniform light source is attenuated by tissue, as simulated with the 7-layer skin model. Furthermore, when the normalized PpIX absorption is used as a weighting factor, the spectral characteristics of effective fluence rates are again modified (Fig. 4B). This fluence rate can be estimated for each light source at a spacing of the 10 µm voxels throughout the depth of the model by

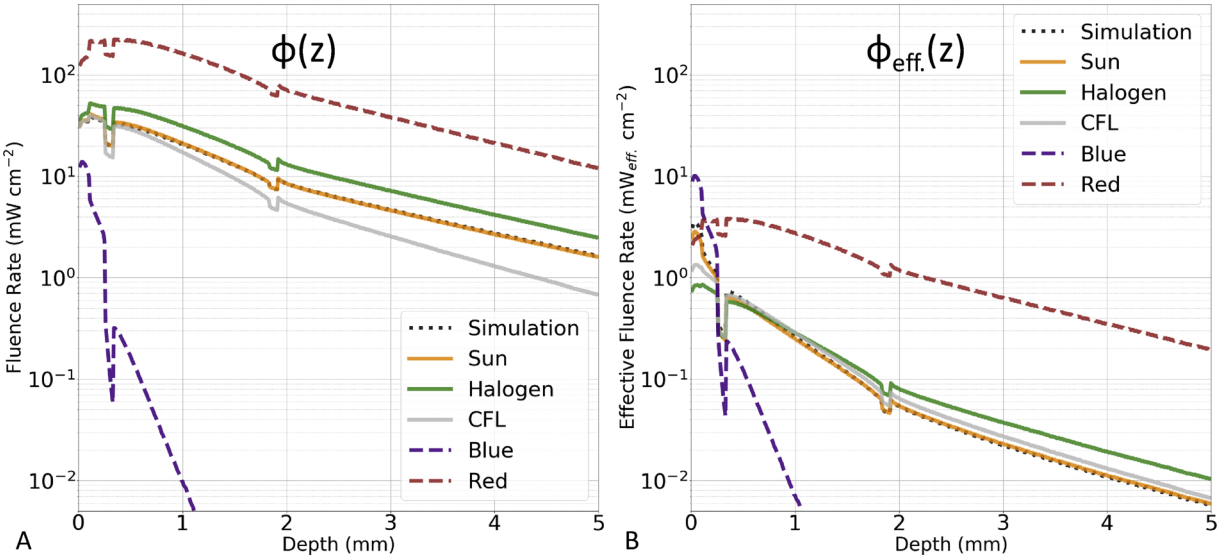


**Fig. 5.** A comparison of the fluence rate (A) and effective fluence rate (B) as a function of depth for the uniform simulation, Sun, CFL, Halogen, Blue LED and Red LED.

summing over the spectral range of interest (350 nm–700 nm). Similarly, the effective fluence rate can be calculated by considering the normalized PpIX absorption weighting factor. The results are the fluence rate and effective fluence rate as a function of depth, φ(z) and $\varphi_{eff}$(z), respectively (Fig. 5).

To determine an appropriate effective threshold fluence, a scalar value ($\zeta_\lambda$) was determined based on the reported central wavelength and assumed a 10 nm or 20 nm full-width half maximum (FWHM) distribution for laser and LED sources, respectively. The scaling can be thought of as the integral of the normalized PpIX spectrum in this spectral range. The PpIX-weighted equivalents of the dose distributions were calculated using (4), where ΔD was first converted to standard deviation ($\sigma_D$). Then the effective pooled standard deviation ($\sigma_{D,eff,pooled}$, 0.2 1 $J_{eff}/cm^2$) was determined using (5). The mean effective threshold fluence (0.06 $J_{eff}/cm^2$) was summed with 3$x$ the effective pooled standard deviation to give the effective fluence threshold (0.70 $J_{eff}/cm^2$) used as shown in Fig. 6.

However, the effective fluence threshold only accounts for the availability of light to activate a sufficient amount of PpIX. Since the photodynamic dose is the product of the light fluence and photosensitizer availability, the PpIX concentration is needed to calculate the threshold photodynamic dose.

The PpIX concentration at depth in the tissue model was found using Eqs. 6–8. The incubation time dictates the initial concentration before photobleaching (8) is considered. Diffusion of the pro-drug during both incubation and treatment allows for deeper PpIX production. Assuming an incubation period of 30 min, which is common in many daylight-PDT protocols, Fig. 7 shows how the PpIX distribution changes over the treatment period, from 30 min to 2 h. The concentration spikes shown in this figure, which are mainly observed in the blue light source, are due to the low-fluence in this tissue layer due to the higher concentration of blood. Using blue-light treatment, with PpIX concentration is higher around 1 mm because of the minimal light penetration, whereas the red-light treatment has lower PpIX

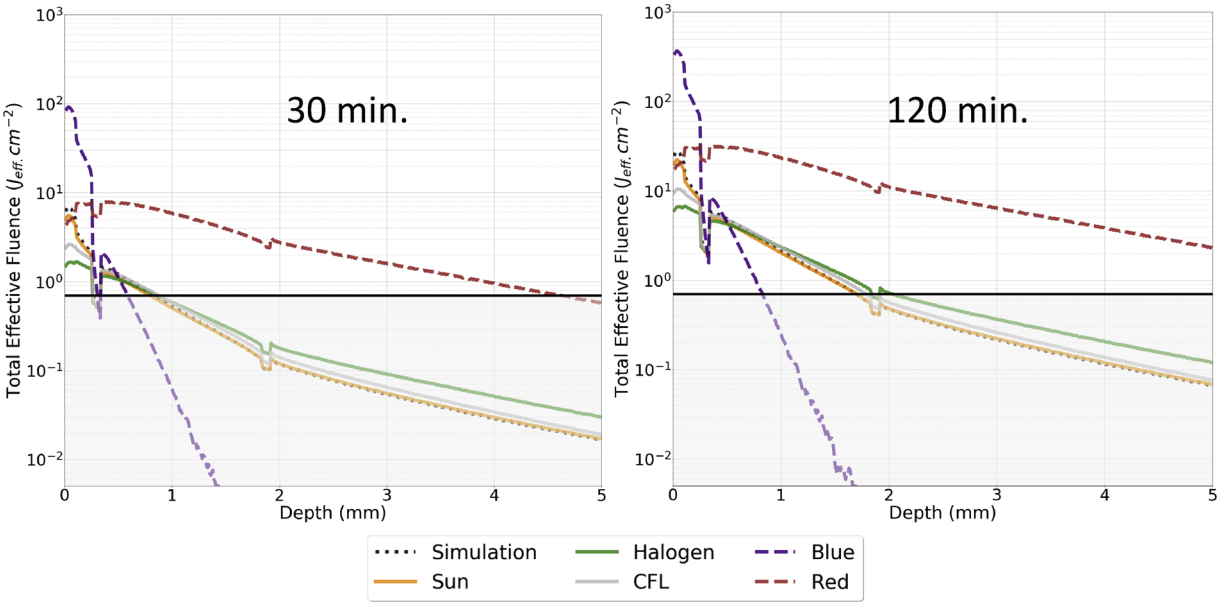


**Fig. 6.** Effective light fluence as a function of time and depth for two different treatment times show how deeper light activation can be achieved by either extending treatment durations or using alternate light sources. The black line shows the expected threshold for PDT response at 0.7 $J_{eff}/cm^2$.

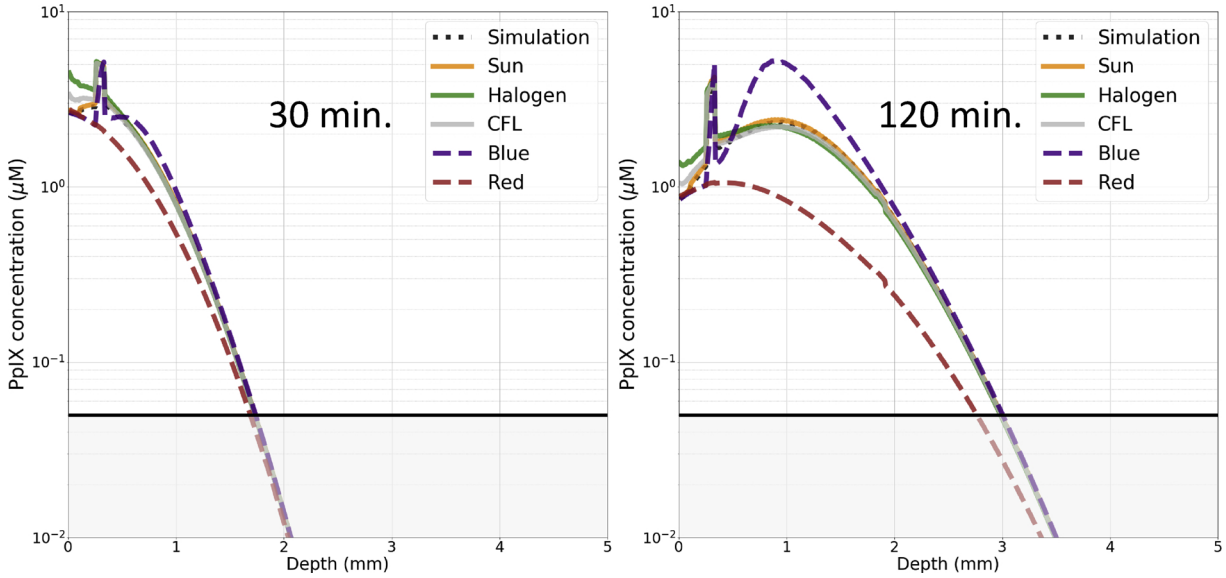


**Fig. 7.** A model of PpIX concentrations at treatement times of 30 min and 2 h for light treatments with a fluence rate of 35 mW/cm$^2$ for broadband sources, and 100 mW/cm$^2$ for the red and blue sources, where both were incubated for 30 min. The black line represents the threshold PpIX concentration (50 nM).

concentrations at depth because the red light is able to propagate further into the tissue and cause additional photobleaching.

A threshold PpIX concentration was considered based on literature reports of *in vitro* and *ex vivo* studies, which indicate effective cell killing can occur when nano-molar concentrations of PpIX are present. [36,37] As a conservative measure, a threshold concentration of 50 nM PpIX was chosen for the current study and is shown as the black line in Fig. 7.

The product of effective fluence threshold ($0.70\,J_{eff}/cm^2$) shown in Fig. 6 and the threshold PpIX concentration (50 nM) was then calculated. The resulting photodynamic dose of 0.035 u M $J_{eff}/cm^2$ is used as the threshold of cytotoxicity for the current study.

Using the effective fluence estimates, PpIX depth distribution and threshold photodynamic dose, the maximal depth of effective PpIX-activated cell death can be tabulated for each source and at various treatment times (Table 3). Even though the light sources investigated have very different effective surface irradiances, over a 20-min treatment window all light sources are able to activate PpIX at a depth of approximately 1 mm, while the blue LED is just shallow of this and the red LED has a much deeper effect. If only the light fluence is considered for all light sources except the red LED, the depth to reach the fluence threshold within 30 min of treatment is approximately 50–60% less than if the photodynamic dose is considered, whereas for the red LED, the opposite is true and the light fluence over-reports the depth of activation by a similar amount.

The duration of the incubation time will impact the initial depth distribution of PpIX. Depending on the spectrum and fluence rate of the treatment light, as well as the duration of light treatment, the PpIX distribution will dynamically change during treatment. Fig. 8 shows a representation of how incubation time and treatment time can impact the depth of activation. Longer incubation and treatment times allow for more PpIX diffusion and result in deeper photodynamic effect. The depth of the threshold photodynamic dose is similar for the 30 min incubation with 2 h treatment, compared to the 2 h incubation with 30 min treatment, however the surface photodynamic dose is slightly higher with the longer incubation.

If the desired depth of activation can be estimated, lookup tables for treatment time needed for cytotoxic effect at various depths can also be tabulated (S4 and summarized in Table 4). The inputs required to generate this table are the light spectrum, fluence rate, incubation time and desired depth of activation. Table 4 shows a representative example of such a lookup table for the Sun spectrum irradiance values typically seen in different seasons, and for incubation times of 5 or 30 min.

## 4. Discussion

As daylight PDT continues to gain clinical adoption, it will be increasingly important to develop a standard for reporting the administered light dose, especially in the settings where the solar spectrum is known to vary. While the actual absorption spectrum used is not yet fully agreed on, resulting in slight variations in effective irradiance estimates reported by different groups [16,18,39], the method of using the normalized PpIX-weighting factor is the first step to improve repeatability, both clinically as well as between studies.

With narrowband excitation performed during conventional PDT, a simple photodiode-based power meter (Thorlabs PM100D) can be used to measure surface irradiance which should remain relatively constant in the clinical setting. However, the increased variability of broad-spectrum irradiance combined with outdoor treatments have led to the introduction of numerous methods to estimate the spectral irradiance. These data collection techniques have utilized wearable photodiodes [21,40–42], regional weather patterns [5,8,22,43,44], lux meters

**Table 3**
Depth (μm) of threshold photodynamic dose for different treatment times after 30 min incubation.

| Light Source | Surface Irradiance (mW/cm$^2$) | Effective Surface Irradiance (mW$_{eff}$/cm$^2$) | *10min* | *20min* | *30min* | *60min* | *90min* | *120min* |
|---|---|---|---|---|---|---|---|---|
| Uniform | 35.0 | 5.0 | 930 | 1170 | 1270 | 1530 | 1720 | 1830 |
| Sun | 35.0 | 4.0 | 920 | 1160 | 1270 | 1530 | 1720 | 1830 |
| CFL | 35.0 | 1.6 | 940 | 1190 | 1290 | 1560 | 1760 | 1900 |
| Halogen | 35.0 | 0.9 | 940 | 1190 | 1310 | 1590 | 1790 | 2000 |
| Blue | 100 | 73.4 | 760 | 880 | 930 | 1030 | 1090 | 1150 |
| Red | 100 | 1.7 | 1260 | 1600 | 1730 | 2100 | 2400 | 2650 |

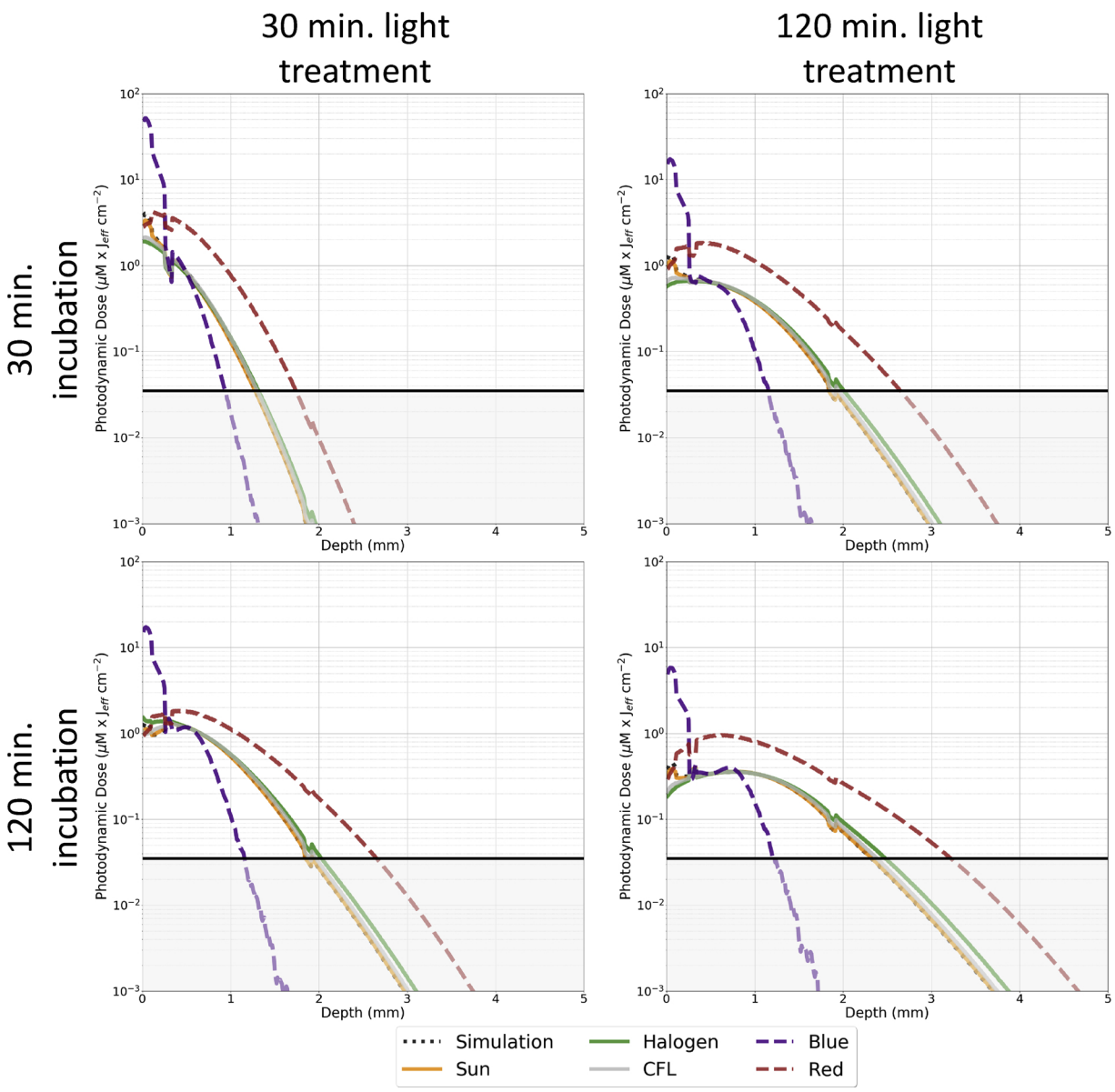


**Fig. 8.** The photodynamic dose will differ between 30 min (left) and 2 h (right) treatments, for incubation tames of 30 min (top) and 2 h (bottom).

[4,9,15], and spectroradiometers [15,18,39], or simply set a treatment time irrespective of the irradiance [45–47].

While a wearable photodiode seems like an ideal solution for the accurate measure of continuous irradiance, placement of the device proximal to the treatment field can be difficult, and wrist-based systems can introduce additional error. Additionally, the ability to acquire a

**Table 4**
Minimum treatment times needed for PpIX-induce cytotoxicity for various Sun irradiance (350 nm–800 nm) values based on uniformly scaled irradiance measurements taken with Apogee SS-110 and reported previously by Marra et al. 18 Yellow-highlighted cells indicate treatment times between 2–2.5 h, whereas red is treatments over 2.5 h. Additional data is provided in S4. (For interpretation of the references to colour in this table legend, the reader is referred to the web version of this article.)

| Source | Irradiance (mW/cm²) | Latitude 45° - 60° Daily Avg.[38] | Effective Irradiance ($mW_{eff}/cm^2$) | Incubation time (min.) | Treatment time (minutes) needed for PDD threshold | | | | | | |
|---|---|---|---|---|---|---|---|---|---|---|---|
| | | | | | 100 μm | 250 μm | 500 μm | 750 μm | 1000 μm | 1500 μm | 2000 μm |
| *Sun* | 10 | Winter | 1.1 | 5 | 1 | 4 | 13 | 26 | 50 | 126 | >210 |
| *Sun* | 10 | | 1.1 | 30 | <1 | 1 | 2 | 11 | 25 | 101 | >210 |
| *Sun* | 30 | Spring, Autumn | 3.4 | 5 | <1 | 2 | 9 | 17 | 33 | 84 | 172 |
| *Sun* | 30 | | 3.4 | 30 | <1 | <1 | 1 | 4 | 13 | 59 | 147 |
| *Sun* | 50 | Summer | 5.7 | 5 | <1 | 1 | 7 | 14 | 27 | 72 | 145 |
| *Sun* | 50 | | 5.7 | 30 | <1 | <1 | 1 | 2 | 11 | 47 | 120 |

commercially available device suitable for the clinic is currently limited. Many groups have turned to weather reports and almanac data to provide a generalized estimate of sunlight available at a given location throughout the year, however transient localized weather confounds the ability to predict treatment times. Illuminance measurements with a lux meter have been used by many groups, but illuminance is a measure of light intensity perceived by the human eye, with a peak sensitivity at 555 nm and a weighting of nearly 0 in the UV/blue region. While there has been work to relate solar irradiance with illuminance measurements [9], the current complexity is prohibitive for most clinical uses. Additionally, illuminance measurements are not ideal for comparing different broadband sources, especially those with a significant UV/blue contribution. We have previously reported collecting continuous measurements using a field-portable spectroradiometer (Apogee SS-110) commonly used in agricultural studies [18]. Measurements of spectrally-resolved irradiance provide the ability to perform PpIX weighting without the introduction of an additional arbitrary weighting inherent in illuminance measurements, however patient positioning relative to the light can still confound results. A study by Manley et al. reported spectroradiometer measurements introduce the least error (13%) when calculating the effective light dose, whereas other methods can introduce 22–83% error [23].

Moving further, the tissue optical properties should be considered in addition to PpIX-weighting when estimating the effective light fluence. Even though the PpIX absorption has already been considered at the surface, other tissue chromophores will absorb and scatter light. This fact is further complicated by broad-spectrum light sources.

In the current study, while equivalent surface irradiance was considered for each broadband light source, the resulting effective irradiance showed up to a 5*x* difference as shown in Fig. 2. Even so, with these substantial differences in effective irradiance at the surface, below the more superficial skin layers (˜250 μm), the effective fluence of these lights are similar. PpIX absorption is not explicitly addressed in the Monte Carlo simulations because of its negligible effect, so instead a normalized PpIX weighting factor is applied. While inter-patient and intra-patient PpIX production can vary greatly, PpIX production was considered based on the work summarized by Campbell. [20] The effective fluence rate within the tissue model can then be used to estimate the photobleaching effect that occurs during treatment. This was combined with the fluence data generated by Monte Carlo simulations to estimate the photodynamic dose.

The multi-layer tissue model provides the ability to define different optical properties due to the stratified anatomy observed in the skin as shown in Figs. 3 & 4 . One result of this stratified model is observed in Figs. 5 & 6, where there are two sharp drops in the fluence rate at depths of 250 μm and 1.83 mm. This is due to the higher concentration of blood assumed in these layers. While modeling the blood content as a thin sheet is an over-simplification of the actual anatomy, it shows how various chromophores concentrations can impact the tissue fluence rates. Additionally, the build-up region after each of these regions can be attributed to the increase in refractive index, as observed between the air and skin surface.

It is worth noting the model for the red LED excitation has a more pronounced buildup region in the most superficial layers of skin than the other light sources, which is expected and was summarized in detail by Moes et al. [48] Due to the dose buildup observed with longer wavelengths, fluence rates at a depth of 150–500 μm are 57% higher than within the first 10 μm. While this higher fluence rate may be able to activate more PpIX, it also results in increased photobleaching, so for long treatments the total photodynamic dose in this range is not greatly increased.

The incident beam size will also impact the tissue fluence rate. This effect is depth-dependent and more pronounced with longer wavelengths, where our model indicates a 21 cm [2] beam at the surface, corresponding to 25 mm radius source, will have 1.1 - 1.7*x* greater fluence within the same voxel space than a beam with surface area of 1 cm [2]. This study used the larger spot size (25 mm radius source) to better simulate field illumination as used in daylight-PDT protocols. While clinically, actual field illumination area may be larger, for this simulation the 21 cm [2] illumination area is sufficiently larger than the 1 cm [2] voxel area used to track photon interactions.

Considering both the available light and the dynamically changing PpIX concentration at depth in tissue, is a complex procedure in clinical practice. The complexity of considering these factors needs to be reduced to a clinically digestible format. To that end, we propose the use of a lookup table that can be used in the clinic to modify light treatments. While Table 3 provides an estimate of the depth of potential PpIX activation as a function of treatment time for each light source considered in the current study, the example in Table 4 is likely more clinically applicable. Since it is likely the light irradiance will fluctuate, Table 4 and S4 provide clinically-relevant dose planning information to define treatment times required to achieve activation at specific depths for each of the light sources over a range of irradiance values and PpIX incubation times. Table 4 also has a column to indicate the seasons most commonly associated with the given irradiance for latitudes between 45° and 60° based on measurements reported by Morton et al, [38] where lower latitudes would have a higher average irradiance. These seasonal variations are based on historical data for specific locations, so daily weather patterns should still be considered when planning daylight-PDT treatments.

The proposed clinical workflow involves the clinician determiing the type of skin lesions that needs treatment and using their judgment to estimate the depth. Using the depth estimate, a specific light source, and a simple measurement of the total irradiance, the information in S4 can be used to estimate a desired incubation and minimum treatment time. If conventional-PDT is desired, longer incubation times with narrowband light sources may be considered, whereas for daylight-PDT shorter incubation times would be used. From these lookup tables it can be observed that blue light is unable to have a photodynamic effect much beyond 1 mm, irrespective of incubation time. However, for deeper lesions (> 1 mm) longer incubation may be required to allow activation within a 2 h window. Ultimately, it is up to the clinician to understand the clinical presentation and determine which light or light combination would be appropriate for treatment. For example, a more superficial AK may benefit from light with additional light dose deposited superficially, whereas a nodular BCC could benefit from a boost of red light to activate PpIX at deeper layers.

While pathology examples presented in Fig. 1 and Table 1 show AK and BCC with depths of less than 500 μm, which according to the lookup table, would take minimal time to treat, it is important to remember the times reported in S4 are to reach the minimum threshold photodynamic dose. So longer treatment times would still be appropriate. While not all the lesions shown in Fig. 1 are commonly treated with PDT, it provides evidence that the effective photodynamic range in tissue could be sufficient to cause some cell death. So further investigations may be appropriate.

Further dermopathologic characterization of AKs and BCCs could help improve the Monte Carlo geometry used in the current study. Chromophore concentrations observed in neoplastic tissues, along with more refined stratification of layers, may prove useful in improving fluence estimates. Additionally, detailed investigation of pro-drug diffusion rates and PpIX production rates in these tissue samples could help better estimate the photodynamic dose.

The lookup tables presented in the present study could be further modified to include factors such as lesion type, estimated depth, melanin content and PpIX production rate. The choice would then be to measure the surface irradiance of a light source with known spectrum and estimate the desired depth of activation. Using these two values the treatment time of a single light source or light combination could then be prescribed. This type of lookup table is something that could easily be included in a web or phone-based application or further automated in a tool used to measure spectral irradiance.

## 5. Conclusions

The current study presented the application of a 7-layer Mote Carlo model to estimate the light fluence in tissue for multiple light sources that have been previously reported for use in PpIX-PDT. The commonly used weighting factor based on the PpIX absorption spectrum was used to find both the effective irradiance at the skin surface as well as the effective fluence rate in tissue. The effective fluence rate was then used to find the total effective fluence for various treatment times. An effective fluence threshold (0. $70 J_{eff}/cm^2$) was introduced based on a meta-analysis of previously published ALA-PpIX induced cell death. The PpIX concentration was estimated for various incubation and treatment durations for a range of fluence rates. Using the product of this fluence threshold and an estimate for the threshold concentration of PpIX (50 nM), a photodynamic dose of 0.035 u M $J_{eff}/cm^2$ is used as the threshold of cytotoxicity. The depth of PpIX-induced cytotoxicity was estimated for various treatment times for each light source at the investigated irradiance values. Even though there was up to a 5*x* reduction between the effective surface irradiance of the broadband light sources, the effective fluence below 250 μm was relatively equivalent. Clinically-relevant lookup tables were introduced to provide a simplified method to estimate treatment times for various light sources over a range of irradiances. From these lookup tables it can be observed that blue light is unable to have a photodynamic effect much beyond 1 mm, irrespective of incubation time. However, for deeper lesions (> 1 mm) longer incubation may be required to allow activation within a 2 h window. The data provided in the lookup tables is compared to clinically relevant histopathology samples to provide context on clinical applications. Moving forward, this model could be extended to include common disease morphologies, melanin contents and PpIX production rates.

## Acknowledgments

This work was funded by the National Institutes of Health and the National Cancer Institute grant P01 CA084203 and by a National Science Foundation Graduate Research Fellowship (EPML).

## Appendix A. Supplementary data

Supplementary material related to this article can be found, in the online version, at https://doi.org/10.1016/j.pdpdt.2019.01.022.

## References

[1] Q. Peng, et al., 5-Aminolevulinic acid-based photodynamic therapy, Cancer 79 (1997) 2282–2308.
[2] L.R. Braathen, et al., Guidelines on the use of photodynamic therapy for non-melanoma skin cancer: an international consensus, J. Am. Acad. Dermatol. 56 (2007) 125–143.
[3] C.A. Morton, R.-M. Szeimies, A. Sidoroff, L.R. Braathen, European guidelines for topical photodynamic therapy part 1: treatment delivery and current indications - actinic keratoses, Bowen's disease, basal cell carcinoma, J. Eur. Acad. Dermatol. Venereol. 27 (2013) 536–544.
[4] S.R. Wiegell, et al., Daylight photodynamic therapy for actinic keratosis: an international consensus, J. Eur. Acad. Dermatol. Venereol. 26 (2012) 673–679.
[5] C.A. Morton, et al., Practical approach to the use of daylight photodynamic therapy with topical methyl aminolevulinate for actinic keratosis: a European consensus, J. Eur. Acad. Dermatol. Venereol. 29 (2015) 1718–1723.
[6] A.-S. Vignion-Dewalle, et al., Photodynamic therapy for actinic keratosis: is the European consensus protocol for daylight PDT superior to conventional protocol for Aktilite CL 128 PDT? J. Photochem. Photobiol. B Biol. 174 (2017) 70–77.
[7] S.R. Wiegell, J. Heydenreich, S. Fabricius, H.C. Wulf, Continuous ultra-low-intensity artificial daylight is not as effective as red LED light in photodynamic therapy of multiple actinic keratoses, Photodermatol. Photoimmunol. Photomed. 27 (2011) 280–285.
[8] L. Spelman, et al., Treatment of face and scalp solar (actinic) keratosis with daylight-mediated photodynamic therapy is possible throughout the year in Australia: evidence from a clinical and meteorological study, Australas. J. Dermatol. 57 (2016) 24–28.
[9] P. O'Mahoney, et al., The use of illuminance as a guide to effective light delivery during daylight PDT in the UK, Br. J. Dermatol. 176 (6) (2017) 1607–1616, https://doi.org/10.1111/bjd.15146.
[10] A.L.R. de Souza, et al., Assessing daylight & low-dose rate photodynamic therapy efficacy, using biomarkers of photophysical, biochemical and biological damage metrics in situ, Photodiagnosis Photodyn. Ther. 20 (2017) 227–233.
[11] 4170 Operating Manual BLU-U ® Blue Light Photodynamic Therapy Illuminator Model 4170 Operating Manual. at http://www.dusapharma.com/assets/files/blu-u-manuals/MAN-1211AW-EN Rev G.pdf.
[12] HE PEAK 415 BLUE LIGHT. at https://www.smarterlights.com/The-Peak-415-Blue-Light-HP-LED-Powerhead-p/e-lt-415.htm.
[13] Omnilux. at http://omniluxled.com/products/omnilux-revive2/.
[14] Tailored for PDT. The reference in LED* lamp technology for PhotoDynamic Therapy (PDT) in Dermatology. at https://www.galderma.se/Portals/3/images/2014/files/Brochure 4p_AKTILITE_201303.pdf.
[15] C. Lerche, I. Heerfordt, J. Heydenreich, H. Wulf, Alternatives to outdoor daylight illumination for photodynamic therapy—use of greenhouses and artificial light sources, Int. J. Mol. Sci. 17 (2016) 309.
[16] S.R. Wiegell, et al., Continuous activation of PpIX by daylight is as effective as and less painful than conventional photodynamic therapy for actinic keratoses; a randomized, controlled, single-blinded study, Br. J. Dermatol. 158 (2008) 740–746.
[17] E. Sotiriou, et al., Daylight photodynamic therapy vs. conventional photodynamic therapy as skin cancer preventive treatment in patients with face and scalp cancerization: an intra-individual comparison study, J. Eur. Acad. Dermatol. Venereol. 31 (8) (2017) 1303–1307, https://doi.org/10.1111/jdv.14177.
[18] K. Marra, et al., Comparison of blue and white lamp light with sunlight for daylight-mediated, 5-ALA photodynamic therapy, in vivo, Photochem. Photobiol. 94 (5) (2018) 1049–1057, https://doi.org/10.1111/php.12923.
[19] Q. Peng, A.M. Soler, T. Warloe, J.M. Nesland, K.-E. Giercksky, Selective distribution of porphyrins in skin thick basal cell carcinoma after topical application of methyl 5-aminolevulinate, J. Photochem. Photobiol. B Biol. 62 (2001) 140–145.
[20] C.L. Campbell, C.T.A. Brown, K. Wood, H. Moseley, Modelling topical photodynamic therapy treatment including the continuous production of Protoporphyrin IX, Phys. Med. Biol. 61 (2016) 7507–7521.
[21] S.R. Wiegell, M. Haedersdal, P. Eriksen, H.C. Wulf, Photodynamic therapy of actinic keratoses with 8% and 16% methyl aminolaevulinate and home-based daylight exposure: a double-blinded randomized clinical trial, Br. J. Dermatol. 160 (2009) 1308–1314.
[22] M.C. Fargnoli, et al., Conventional vs. daylight methyl aminolevulinate photodynamic therapy for actinic keratosis of the face and scalp: an intra-patient, prospective, comparison study in Italy, J. Eur. Acad. Dermatol. Venereol. 29 (2015) 1926–1932.
[23] M. Manley, P. Collins, L. Gray, S. O'Gorman, J. McCavana, Quantifying the radiant exposure and effective dose in patients treated for actinic keratoses with topical photodynamic therapy using daylight and LED white light, Phys. Med. Biol. 63 (3) (2018) 035013, https://doi.org/10.1088/1361-6560/aa9ea7.
[24] M. Taniguchi, J.S. Lindsey, Database of absorption and fluorescence spectra of &300 common compounds for use in PhotochemCAD, Photochem. Photobiol. 94 (2018) 290–327.
[25] R.M. Valentine, C.T.A. Brown, H. Moseley, S. Ibbotson, K. Wood, Monte Carlo modeling of in vivo protoporphyrin IX fluorescence and singlet oxygen production during photodynamic therapy for patients presenting with superficial basal cell carcinomas, J. Biomed. Opt. 16 (2011) 048002.
[26] B. Liu, T.J. Farrell, M.S. Patterson, Comparison of photodynamic therapy with different excitation wavelengths using a dynamic model of aminolevulinic acid-photodynamic therapy of human skin, J. Biomed. Opt. 17 (2012) 0880011.
[27] C.L. Campbell, K. Wood, R.M. Valentine, C.T.A. Brown, H. Moseley, Monte Carlo modelling of daylight activated photodynamic therapy, Phys. Med. Biol. 60 (2015) 4059–4073.
[28] P. Arce, P. Rato, M. Canadas, J.I. Lagares, GAMOS: a Geant4-based easy and flexible framework for nuclear medicine applications, 2008 IEEE Nuclear Science Symposium Conference Record 3162–3168 (2008), https://doi.org/10.1109/NSSMIC.2008.4775023.
[29] P. Arce, et al., Gamos: a framework to do Geant4 simulations in different physics fields with an user-friendly interface, Nucl. Instruments Methods Phys. Res. Sect. A Accel. Spectrometers, Detect. Assoc. Equip. 735 (2014) 304–313.
[30] I.V. Meglinski, S.J. Matcher, Quantitative assessment of skin layers absorption and skin reflectance spectra simulation in the visible and near-infrared spectral regions, Physiol. Meas. 23 (2002) 741–753.
[31] A.K. Glaser, S.C. Kanick, R. Zhang, P. Arce, B.W. Pogue, A GAMOS plug-in for GEANT4 based Monte Carlo simulation of radiation-induced light transport in biological media, Biomed. Opt. Express 4 (2013) 741–759.
[32] J. Berlanda, T. Kiesslich, V. Engelhardt, B. Krammer, K. Plaetzer, Comparative in vitro study on the characteristics of different photosensitizers employed in PDT, J. Photochem. Photobiol. B Biol. 100 (2010) 173–180.
[33] A. Casas, et al., Tumor cell lines resistant to ALA-mediated photodynamic therapy and possible tools to target surviving cells, Int. J. Oncol. 29 (2006) 397–405.
[34] B.A. Hartl, H. Hirschberg, L. Marcu, S.R. Cherry, Characterizing low fluence thresholds for in vitro photodynamic therapy, Biomed. Opt. Express 6 (2015) 770.
[35] C.M.G. de Faria, N.M. Inada, C. Kurachi, V.S. Bagnato, Determination of the threshold dose distribution in photodynamic action from in vitro experiments, J. Photochem. Photobiol. B, Biol. 162 (2016) 168–175.
[36] L. Schmitz, B. Novak, A.-K. Hoeh, H. Luebbert, T. Dirschka, Epidermal penetration and protoporphyrin IX formation of two different 5-aminolevulinic acid formulations in ex vivo human skin, Photodiagnosis Photodyn. Ther. 14 (2016) 40–46.
[37] B. Novak, L. Heesen, N. Schary, H. Lübbert, The influence of different illumination parameters on protoporphyrin IX induced cell death in squamous cell carcinoma cells, Photodiagnosis Photodyn. Ther. 21 (2018) 385–392.

[38] C.A. Morton, et al., Practical approach to the use of daylight photodynamic therapy with topical methyl aminolevulinate for actinic keratosis: a European consensus, J. Eur. Acad. Dermatol. Venereol. 29 (2015) 1718–1723.
[39] D.M. Rubel, et al., Daylight photodynamic therapy with methyl aminolevulinate cream as a convenient, similarly effective, nearly painless alternative to conventional photodynamic therapy in actinic keratosis treatment: a randomized controlled trial, Br. J. Dermatol. 171 (2014) 1164–1171.
[40] E. Thieden, M.S. Agren, H.C. Wulf, The wrist is a reliable body site for personal dosimetry of ultraviolet radiation, Photodermatol. Photoimmunol. Photomed. 16 (2000) 57–61.
[41] J. Heydenreich, H.C. Wulf, Miniature personal electronic UVR dosimeter with erythema response and time-stamped readings in a wristwatch, Photochem. Photobiol. 81 (2005) 1138.
[42] S.R. Wiegell, et al., A randomized, multicentre study of directed daylight exposure times of 1½ vs. 2½ h in daylight-mediated photodynamic therapy with methyl aminolaevulinate in patients with multiple thin actinic keratoses of the face and scalp, Br. J. Dermatol. 164 (2011) 1083–1090.
[43] B. Grinblat, et al., Feasibility of daylight-mediated photodynamic therapy for actinic keratosis throughout the year in Central and South America: a meteorological study, Int. J. Dermatol. 55 (2016) e488–e493.
[44] J.-A. See, et al., Consensus recommendations on the use of daylight photodynamic therapy with methyl aminolevulinate cream for actinic keratoses in Australia, Australas. J. Dermatol. 57 (2016) 167–174.
[45] L. Braathen, Daylight photodynamic therapy in private practice in Switzerland: gain without pain, Acta Derm. Venereol. 92 (2012) 652–653.
[46] N. Neittaanmäki-Perttu, T.T. Karppinen, M. Grönroos, T.T. Tani, E. Snellman, Daylight photodynamic therapy for actinic keratoses: a randomized double-blinded nonsponsored prospective study comparing 5-aminolaevulinic acid nanoemulsion (BF-200) with methyl-5-aminolaevulinate, Br. J. Dermatol. 171 (2014) 1172–1180.
[47] J.-P. Lacour, et al., Daylight photodynamic therapy with methyl aminolevulinate cream is effective and nearly painless in treating actinic keratoses: a randomised, investigator-blinded, controlled, phase III study throughout Europe, J. Eur. Acad. Dermatol. Venereol. 29 (2015) 2342–2348.
[48] C.J. Moes, M.J. van Gemert, W.M. Star, J.P. Marijnissen, Sa. Prahl, Measurements and calculations of the energy fluence rate in a scattering and absorbing phantom at 633 nm, Appl. Opt. 28 (1989) 2292–2296.